Saturation of the Magnetic Response of Split-Ring Resonators at Optical Frequencies

J. Zhou,[1] Th. Koschny,[1,2] M. Kafesaki,[2,3] E. N. Economou,[2,4] J. B. Pendry,[5] and C. M. Soukoulis[1,2,3]

[1]*Ames Laboratory and Department of Physics and Astronomy, Iowa State University, Ames, Iowa 50011, USA*
[2]*Institute of Electronic Structure and Laser, FORTH, 71110 Heraklion, Crete, Greece*
[3]*Department of Materials Science and Technology, University of Crete, Greece*
[4]*Department of Physics, University of Crete, Greece*
[5]*Condensed Matter Theory Group, The Blackett Laboratory, Imperial College, London SW7 2BZ, United Kingdom*

(Received 18 July 2005; published 23 November 2005)

We investigate numerically the limits of the resonant magnetic response with a negative effective permeability μ_{eff} for single-ring multicut split-ring resonator (SRR) designs up to optical frequencies. We find the breakdown of linear scaling due to the free electron kinetic energy for frequencies above $\sim$100 THz. Above the linear scaling regime, the resonance frequency saturates, while the amplitude of the resonant permeability decreases, ultimately ceasing to reach negative value. The highest resonance frequency at which $\mu_{\text{eff}} < 0$ increases with the number of cuts in the SRR. A *LC* circuit model provides explanation of the numerical data.

DOI: 10.1103/PhysRevLett.95.223902 PACS numbers: 42.70.Qs, 41.20.Jb, 42.25.Bs, 73.20.Mf

In the past few years, left-handed metamaterials (LHMs) of the split-ring resonator (SRR) [1] plus continuous wire [1] type have been intensely studied throughout a wide window of operating frequencies, from radio and microwaves [2,3] up to the THz region [4–7]. In some narrow frequency band, the key components SRR and wire simultaneously provide a negative effective permeability μ_{eff} (due to a resonance of circular currents around the SRR) and a negative effective permittivity ε_{eff} with plasma frequency ω_p' greatly reduced compared to that of bulk metal ω_p, as a result mainly of the magnetic field energy dominating the kinetic energy of the current carrying electrons (for frequencies much lower than 100 THz). The antiparallel Poynting and wave vector exhibited by LHMs enables a range of interesting possible applications, such as negative refraction, superlensing [8], etc.

There is a sustained effort [4–7,9] in the community to push the operating frequency of the metamaterials deeper and deeper into the THz region to reach ultimately optical frequencies. This is so important because there are no natural materials that have magnetic properties at such high frequencies. At low frequency regimes, up to several THz, the magnetic resonance frequency scales reciprocally with the structural size. At high frequencies, however, this linear scaling breaks down, as we show in this Letter. Although, in principle, the dielectric materials could also show an explicit frequency dependence of their material parameters, it is the metal that first limits the operation of the SRRs. At high frequencies, the kinetic energy of the electrons in the metal (in both the SRRs and the wires) cannot be neglected anymore in comparison with the magnetic energy. Indeed, the kinetic energy of the electrons in the SRR adds to the magnetic energy a term which can be written as $L_e I^2/2$, where the electron self-inductance L_e is given by $l'/(S'\omega_p^2\varepsilon_0)$, where $l' = 4(l - w) - d$ is the length of the axis of the wire making the ring (see Fig. 1); S' is the effective cross section of the ring, smaller than $S = wt$ (because of the skin depth and the asymmetry of the current distribution between the center and the external sides of the ring), and ω_p is the plasma frequency of the material. The geometrical parameters l, w, and d are defined in Fig. 1, along with their values for the SRR systems studied here.

The formula $L_e = l'/(S'\omega_p^2\varepsilon_0)$ can be derived in a straightforward way by taking into account that the elec-

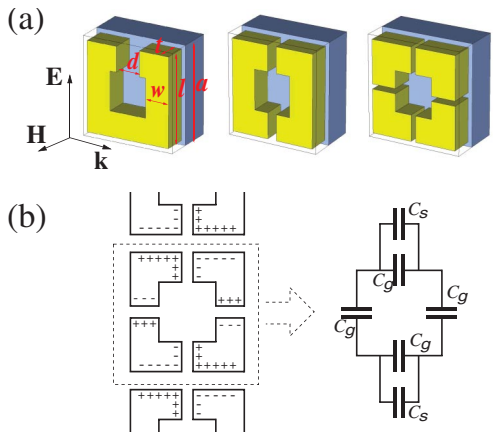

FIG. 1 (color online). (a) The geometries of the 1-, 2-, and 4-cut single-ring SRRs are shown; the unit cell has the dimensions $a \times a$ in the SRR plane and $0.614a$ perpendicular to it. The SRR is made of aluminum, simulated using a Drude-model permittivity ($f_p = \omega_p/2\pi = 3570$ THz, $f_\tau = 19.4$ THz), separated from the $0.343a$ thick substrate (glass, $\varepsilon = 2.14$) by a $0.014a$ thin indium tin oxide layer ($\varepsilon = 7$). The parameters of the SRR are side length $l = 0.914a$, width and thickness $w = t = 0.257a$, and cut width (d) $0.2a$, $0.1a$, and $0.05a$ for the 1-, 2-, and 4-cut SRRs, respectively. (b) The left panel shows the charge accumulation in a 4-cut SRR, as a result of the periodic boundary conditions in the $\vec{E}$ (and $\vec{H}$) direction. The right panel shows the equivalent *LC* circuit describing this SRR. C_g is the gap capacitance and C_s the side capacitance resulting from the interaction with the neighboring SRR.

tronic kinetic energy $L_e I^2/2$ is $N_e m_e v_e^2/2$, where $v_e = j_e/(en_e)$, $I = \int ds j_e = S' j_e$, v_e is the average electron velocity, j_e is the current density, n_e is the free electron concentration, $N_e = l' S' n_e$ is the total number of electrons participating in the current, and $S' = \gamma S$, with $\gamma < 1$. Notice that L_e scales as $1/a$, where a is the unit cell size in the SRR plane, in contrast to the magnetic field inductance L_m, which scales as a. The capacitance C of the split ring scales also proportional to a (since all the geometrical features scale proportional to a), so that the resonance frequency f_m of the SRR has the following a dependence:

$$f_m = \frac{1}{2\pi} \frac{1}{\sqrt{(L_m + L_e)C}} = \frac{1}{2\pi} \frac{1}{\sqrt{c_1 a^2 + c_2}}, \qquad (1)$$

where c_1 and c_2 are independent of the length a in the framework of the LC circuit model. For very small structural sizes, i.e., high frequencies, other factors that break the linear scaling and contribute to the increase of the Ohmic losses are the increased scattering of electrons at the surface of the metal and the larger skin depth over metal thickness ratio (note that the skin depth scales as $1/\sqrt{a}$, i.e., slower than $1/a$). In contrast to the electron self-inductance L_e, those two effects depend in a complicated way on the geometry and, in the experiment, also on the surface smoothness, which prevents us from a more detailed analysis of their effect.

Taking everything together, as we push the magnetic resonance frequency higher by reducing the structural size of the SRR, we expect to see a breakdown of the linear scaling, which, together with a diminishing strength of the SRR resonance due to the increase of the losses, ultimately renders the SRR dysfunctional.

In this Letter, we investigate how high we can push the magnetic resonance frequency of a realistic SRR design made from aluminum. As shown in Fig. 1, we have considered single-ring (and not double-ring) SRRs as well as multicut SRRs. There are several important advantages of these choices. Theoretical and experimental studies [6,7] have proved that an effective SRR can be built from a single-ring design exploiting only the capacitance across and near the cuts; this simplifies the fabrication, especially for small structural sizes, and potentially reduces dielectric losses, since the fields get strong only in and around the cuts but not between the rings anymore. Keeping in mind the need for higher dimensional *isotropic* metamaterials, the unit cell has to be symmetric; hence, in turn, a symmetric SRR design [10] is required, as the 4-cut one; this, as the 2-cut one, avoids the undesirable excitation of the magnetic resonance by the electric field [11,12].

We simulate single-ring SRR-only metamaterial designs similar to the experimental samples previously employed in the 100 THz frequency range [5] for near infrared and optical frequencies, using the commercial MICROWAVE STUDIO code. The metamaterial is defined as a periodic repetition of a single rectangular unit cell containing a single SRR, as shown in Fig. 1. The cut size has been reduced according to the number of cuts, expecting to approximately preserve the total capacitance C and the total inductance L_m of the effective LC circuit constituted by the SRR (assuming that $C \sim wt/d$ and $L_m \sim l'$). The direction of propagation and the electric field are parallel to the SRR plane. The orientation of the SRR is such that mirror symmetry with respect to the electric field vector is preserved; thus, only the magnetic field couples to the resonance of the circular currents in the SRR ring.

The purpose of the SRR metamaterial is to provide an effective *homogeneous* negative magnetic permeability, $\mu_{\text{eff}} < 0$. This is guaranteed only in the limit where the unit cell is much smaller than the wavelength of the electromagnetic radiation. For realistic unit cells, we see artifacts in the homogeneous medium approximation brought about by the periodicity [13,14], such as resonance-antiresonance coupling between μ_{eff} and ε_{eff} or negative imaginary parts in ε_{eff}. These artifacts basically occur when the wavelength inside the material becomes comparable with the size of the unit cell, i.e., when the effective index of refraction n_{eff} renders the wave vector close to the edge of the Brillouin zone and periodicity band gaps appear intermixed with the generic behavior of the resonance.

In Fig. 2, we show the results of our simulation for f_m, together with the outcome of the LC circuit model, Eq. (1). It is worthwhile to point out that the simple formula (1) with realistic values of c_1 and c_2 reproduces well the simulation, especially for the 4- and the 1-cut cases; the saturation value of the 2-cut case is lower than the simulation value by 19%; this discrepancy is attributed to a breakdown of the homogeneous effective medium (see below). On the basis of the simple formulas $C \sim wt/d$ and $L_m \sim l'$, it is expected that the three simulation curves ought to more or less coincide, since l' is the same for the 1-, 2-, and 4-cut cases and $C_2 = C_4 = C$,

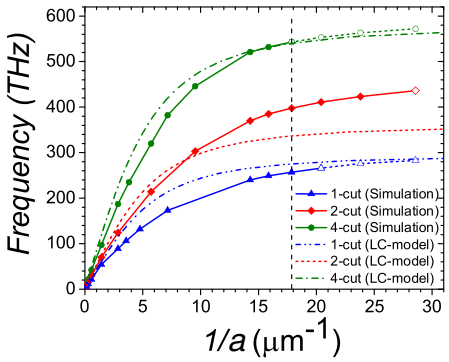

FIG. 2 (color online). The scaling of the *simulated* magnetic resonance frequency f_m as a function of the linear size a of the unit cell for the 1-, 2-, and 4-cut SRRs (solid lines with symbols). Up to the lower terahertz region, the scaling is linear, $f_m \propto 1/a$. The maximum attainable frequency is strongly enhanced with the number of cuts in the SRR ring. The hollow symbols as well as the vertical line at $1/a = 17.9\ \mu\text{m}^{-1}$ indicate that no $\mu < 0$ is reached anymore. The nonsolid lines show the scaling of f_m calculated through Eq. (1) (LC circuit model).

since $C_2 = Cd/(2d_2)$, $C_4 = Cd/(4d_4)$, and $d_2 = d/2$ and $d_4 = d/4$ (the subscript in capacitance and cut width refers to the 2- and 4-cut cases). However, as is shown in Fig. 2, the ratio of the f_ms in the linear regime is $f_{m,2}/f_{m,1} = 1.39$, $f_{m,4}/f_{m,1} = 2.1$, which implies, assuming $L_{m,4} \approx L_{m,2} \approx L_{m,1}$, that $C_1/C_4 = 4.4$ and $C_1/C_2 = 1.93$. There are two physical reasons why those ratios are so different from one. First, the formula $C \sim wt/d$ is not valid because d is not much smaller than w. Numerical electrostatic calculation of the capacitance (approximately including the presence of the dielectric substrate) *at each cut* gives $C_g^{(1)} = 10.5a$ pF, $C_g^{(2)} = 12.7a$ pF, and $C_g^{(4)} = 18a$ pf (a in meters), where the superscript refers to the 1-, 2-, and 4-cut cases, respectively. Second, because of the periodic boundary conditions along the direction of the electric field only (in the simulations, there is only one unit cell along the $\vec{k}$ direction), there is a charge accumulation to the sides of the cuts, as shown in Fig. 1(b) for the 4-cut case. This adds a side capacitance $C_s^{(n)}$, $n = 1, 2, 4$, which was found numerically to be (including an estimated increase due to the dielectric substrate) $C_s^{(1)} = 13.109a$ pF, $C_s^{(2)} = 18.81a$ pF, and $C_s^{(4)} = 20.22a$ pF (a in meters). Combining these values [see Fig. 1(b)], we found $C_1 = 23.609a$ pF, $C_2 = 15.755a$ pF, and $C_4 = 6.118a$ pF. The ratios of the electrostatically calculated capacitances $C_1/C_4 = 3.86$ and $C_1/C_2 = 1.50$ turn out to be lower than, but not far from, the ones inferred from the simulations. The difference can be attributed to the previously mentioned approximations in obtaining the various L and C and to retardation effects present in the simulation but absent in the LC circuit modeling.

We calculated also the inductance $L_m = L_m^{(\mathrm{out})} + L_m^{(\mathrm{in})}$ by employing the formulas [15] $L_m^{(\mathrm{out})} = (\mu_0 l'/2\pi) \times [\log(8r/b) - 1.75]$ (inductance of a circular ring of radius r, with a circular cross section of radius b), where $r = l'/2\pi$, $\pi b^2 = wt$ and $l' = 4(l - w) - d$ for the inductance outside the metal and $L_m^{(\mathrm{in})} = (\mu_0 l'/8\pi)$ for the internal inductance in the metal. The final result is $L_m = 0.76a$ μH (a in meters). In obtaining these values, we have ignored the mutual inductance due to the periodicity along the $\vec{H}$ direction (see Fig. 1) because of the rather large separation ($0.614a$); on the other hand, we corrected the above values, taking into account that the periodic boundary conditions (along the direction of the electric field) imply mutual inductances which reduce the value of L_m by a factor estimated to be 0.75. Thus, $L'_m = 0.75L_m = 0.57a$ μH (a in meters).

Using the formula for L_e derived before (with $\gamma = 2/3$) and the total capacitance values, we find the c_2 of Eq. (1); for the 1-cut case, $c_2 = 0.29 \times 10^{-30}$. Using our numerical results, Eq. (1) is reduced to

$$f_m^{(n)} = \frac{159 \text{ THz}}{\sqrt{c'_n}\sqrt{6.43a^2 + 0.14}}, \qquad n = 1, 2, 4, \qquad (2)$$

where a is in μm, and $c'_1 = 2.08$, $c'_2 = 1.39$, $c'_4 = 0.54$.

We expect the magnetic resonance to become broader and weaker for each of the three cases studied here as the size becomes smaller and the resonance frequency increases; this is due to the losses that are increasing linearly with the resonance frequency. Furthermore, the permittivity of the metal, described in our simulations through the Drude-model formula, becomes smaller as the frequency increases, and, hence, the contrast to vacuum decreases, while Ohmic losses are increasing, leading to a weaker resonance of the SRR. The permittivity of the dielectrics is still considered frequency independent in our simulations, using its typical values in the THz regime.

The transition to everywhere positive $\mathrm{Re}\mu(\omega)$ is indicated by the change from full to hollow symbols in Fig. 2. Interestingly, this transition occurs pretty consistently for all SRR designs for a specific size around 50 nm rather than for a specific frequency. This behavior can be deduced from the LC circuit analysis. Indeed, one can obtain a rough estimate of the permeability $\mu = \mu_0(1 + \chi)$, where χ is the magnetic susceptibility. Using the well known formulas $\chi = M/H = m/VH$, $m = IA$, $I = E/Z$, and $E = -d\Phi/dt = i\omega\mu HA$, where M is the magnetization, m is the magnetic moment of the unit cell of volume V, $H = B/\mu$, B is the magnetic field, I is the current, $A = l'^2$ is the area of the loop, Φ is the magnetic flux through the loop, Z is the impedance, $Z = R + iL_t\omega[1 - (\omega_m/\omega)^2]$, $R = \rho l'/S'$, $\rho = 1/\sigma$, where $\sigma = -i\omega(\varepsilon - \varepsilon_0)$ is the ac conductivity given by the Drude formula, and $L_t = L_m + L_e$. The final result is of the form $\chi = \Lambda/(1 - \Lambda)$, where Λ for $\omega \approx \omega_m$ and $\omega_m \gg \omega_\tau$ turns out to be independent of ω_m and proportional to length square. On the other hand, the LC circuit model gives $|\chi|$ always less than unity, which means μ_{eff} positive, in disagreement with the simulations and the experiment.

In Fig. 3, we show the disappearance of the $\mu_{\mathrm{eff}} < 0$ region in the magnetic response with decreasing structure size for the 4-cut SRR design. The effective permeability $\mu_{\mathrm{eff}}(\omega)$ has been obtained by employing the retrieval procedure [16] from the simulated scattering data. Qualitatively, as we pointed out before, with decreasing size of the unit cell, ω_m moves to higher frequencies but slower than it would be expected from the linear scaling. Simultaneously, the strength of the resonance, and, hence, the amplitude of the resonant μ_{eff}, decreases. Starting from $\mu_{\mathrm{eff}} \approx 1$ far from ω_m, a weak resonant μ_{eff} cannot reach negative values anymore, although the presence of the magnetic resonance can be confirmed up to very small unit cells. However, even in those cases, which are uninteresting for constructing left-handed metamaterials, the resonance frequency does not significantly increase by decreasing the structural size. It must be stressed that the 4-cut design retains the negative $\mathrm{Re}\mu$ region for higher frequencies (up to about 550 THz) than the 2-cut design (up to 420 THz) and the 1-cut case (up to 280 THz). The explanation for this superior performance of the 4-cut case can be inferred from the dependence of the frequency of the disappearance of the negative μ regime mainly on the

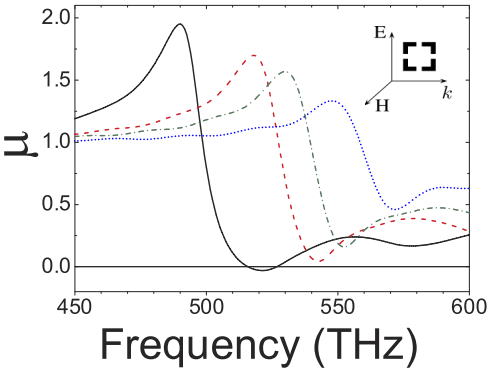

FIG. 3 (color online). Simulation of the shape and amplitude of the magnetic resonance in $\mathrm{Re}\mu(\omega)$ of the 4-cut SRR for unit cell size $a = 70$, 56, 49, and 35 nm (left to right).

length scale and the fact that more cuts of smaller widths produce higher electric field gradients [17], smaller capacitances, and, hence, higher magnetic resonance frequency for the same length scale. The 2-cut case needs further discussion. For a given structural size, the resonance frequency ω_m increases with the number of cuts, which brings the resonant refractive index n_{eff} closer in frequency to the edge of the Brillouin zone, $n_{\mathrm{BZ}} = \pi c/\omega a$, promoting periodicity artifacts. In contrast, two effects counteract the periodicity: Generally, the breakdown of the linear scaling limits the increase of ω_m, while the edge of the Brillouin zone continues to scale geometrically, leading to reduced periodicity artifacts deeper in the saturation regime, i.e., for smaller structural size. Second, the increasing losses at higher frequencies reduce the amplitude of the magnetic resonance and increase the separation of the resonant n_{eff} from the n_{BZ} in the vertical direction (i.e., in magnitude) despite a smaller $\lambda_{\mathrm{vacuum}}/a$ ratio. Consequently, we see a very weak periodicity artifact for the single-cut SRR, becoming strong for the 2-cut SRR but decreasing again for the 4-cut SRR. The periodicity leads to a deformation of the μ_{eff} resonance, as has been discussed in great detail in Ref. [13], which saturates and widens the $\mu_{\mathrm{eff}} < 0$ region.

We stress the fact that the 4-cut single-ring SRR design is favorable for more-dimensional metamaterials not only for its highest attainable magnetic resonance frequency but also for its inherent symmetry [11,12]. For the 2-cut design, the role of elongating the two noncut sides is worthwhile to be explored, since this way one may induce a negative ε response as well.

In conclusion, we investigated numerically the limits of the resonant magnetic response with negative effective permeability $\mu_{\mathrm{eff}} < 0$ for realistic single-ring multicut SRR designs at optical frequencies. We found the breakdown of linear scaling due to the increasing importance of the kinetic energy of the conduction electrons. The magnetic resonance of the SRR is traceable down to a very small structural size of $\sim$35 nm; however, the resonance frequency saturates above the linear scaling regime, while the amplitude of the resonant permeability decreases, ultimately ceasing to reach negative value. The highest possible resonance frequency exhibiting $\mu_{\mathrm{eff}} < 0$ strongly increases with the number of cuts in the SRR and depends mainly on the length scale, disappearing for $a \approx 60$ nm. The simulation results can be explained by a LC circuit model, which reproduces the quantitative aspects of the resonance frequency vs length scale, especially for the 4-cut and the 1-cut cases. The discrepancy for the 2-cut case can possibly be attributed to the complications by periodicity artifacts, which, at larger structure size, increase with the number of cuts in the SRR but for small structural size, deep in the saturation limit, become less important again. It would be interesting to test our predictions by fabricating the 4-cut rings using gold and silver (which exhibit lower losses and closer to Drude-model behavior even at very high frequencies).

This work was partially supported by Ames Laboratory (Contract No. W-7405-Eng-82), financial support by EU-projects DALHM, Metamorphose, Phoremost and Molecular Imaging, by DARPA (Contract No. HR0011-05-C-0068) and by Greek Ministry of Education (PYTHAGORAS project).

[1] J. B. Pendry, A. J. Holden, D. J. Robbins, and W. J. Stewart, IEEE Trans. Microwave Theory Tech. **47**, 2075 (1999); J. Phys. Condens. Matter **10**, 4785 (1998).
[2] D. R. Smith *et al.*, Phys. Rev. Lett. **84**, 4184 (2000).
[3] R. A. Shelby *et al.*, Science **292**, 77 (2001); Appl. Phys. Lett. **78**, 489 (2001).
[4] T. J. Yen *et al.*, Science **303**, 1494 (2004).
[5] S. Linden, C. Enkrich, M. Wegener, J. Zhou, T. Koschny, C. M. Soukoulis, Science **306**, 1351 (2004).
[6] S. O'Brien, D. McPeake, S. A. Ramakrishna, and J. B. Pendry, Phys. Rev. B **69**, 241101(R) (2004).
[7] N. Katsarakis *et al.*, Opt. Lett. **30**, 1348 (2005).
[8] J. B. Pendry, Phys. Rev. Lett. **85**, 3966 (2000).
[9] V. A. Podolskiy, A. K. Sarychev, and V. M. Shalaev, J. Nonlinear Opt. Phys. Mater. **11**, 65 (2002).
[10] T. Koschny, L. Zhang, and C. M. Soukoulis, Phys. Rev. B **71**, 121103(R) (2005).
[11] N. Katsarakis, T. Koschny, M. Kafesaki, E. N. Economou, and C. M. Soukoulis, Appl. Phys. Lett. **84**, 2943 (2004).
[12] R. Marqués, F. Medina, and R. Rafii-El-Idrissi, Phys. Rev. B **65**, 144440 (2002).
[13] T. Koschny *et al.*, Phys. Rev. B **71**, 245105 (2005).
[14] T. Koschny, P. Markoš, D. R. Smith, and C. M. Soukoulis, Phys. Rev. E **68**, 065602(R) (2003).
[15] L. D. Landau and E. M. Lifshitz, *Electrodynamics of Continuous Media* (Pergamon, Oxford, 1984).
[16] D. R. Smith *et al.*, Phys. Rev. E **71**, 036617 (2005).
[17] A. B. Movchan and S. Guenneau, Phys. Rev. B **70**, 125116 (2004).